BMC Chemistry

RESEARCH

Open Access

Exploring green solvent systems and enhanced solubility of xanthone in triglyceride-based tricaprin-tricaprylin mixtures with thermodynamic insights

Hua Liu[1,2], Johnson Stanslas[3], Jiaoyan Ren[4], Norhidayah Binti Suleiman[1] and Gun Hean Chong[1*]

Abstract

This study explores the use of green solvent systems by investigating the solubility and thermodynamic properties of xanthone (1) in triglyceride-based tricaprin (2) and tricaprylin (3) mixtures, aiming to replace traditional organic solvents. The solubility profile exhibited a concave trend, and the highest solubility was observed at a solute-free fraction (x_2) of 0.36. The solubility exponentially increased with increasing temperature in the range from 30 °C to 75 °C. The solubility data were effectively correlated using the local composition-regular solution theory (LC-RST) model and achieved an ARDln value of 4.8×10^{-3}. The model indicated strong interactions between tricaprin and tricaprylin, followed by interactions between tricaprylin and xanthone and between tricaprin and xanthone. The dissolution process of xanthone was primarily enthalpy driven. Based on the structural analysis, xanthone maintained its molecular structure after dissolution in tricaprin and tricaprylin; however, changes in crystallinity levels were observed. These findings provide insights into the use of triglycerides as solvents to improve the solubility and bioaccessibility of hydrophobic compounds such as xanthone.

Keywords Xanthone, Medium-chain triglyceride, Solubility, Thermodynamic model

Introduction

The mangosteen (*Garcinia mangostana*) is a tropical fruit native to Southeast Asia, and the mangosteen pericarp (MP) has long been valued for its medicinal properties. Traditionally, MP has been used to treat various ailments, including diarrhoea, abdominal pain, and dysentery, and as a topical treatment for burns, bruises, sprains, and wound infections [1]. Scientific studies have also reported the health benefits of the MP extracts. This extract is rich in xanthones and their derivatives; xanthones are a class of polyphenolic compounds. These compounds exhibit a wide range of biological activities, including antioxidation, anticancer, anti-AIDS, anti-inflammatory, antiviral, antibacterial, and antiallergenic effects [2–5]. Despite their promising therapeutic potential, the extraction and utilization of xanthones has considerable challenges. Traditional extraction methods often involve organic solvents [6], and supercritical carbon dioxide ($scCO_2$) extraction has also been explored [7]. However, these methods have limitations, particularly in terms of extraction efficiency and the extremely low water solubility of

*Correspondence:
Gun Hean Chong
gunhean@upm.edu.my
[1] Food Science and Technology, Universiti Putra Malaysia, 43400 Serdang, Malaysia
[2] Guangzhou College of Technology and Business, GuangZhou 510850, China
[3] Medicine and Health Sciences, Universiti Putra Malaysia, 43400 Serdang, Malaysia
[4] Food Science and Engineering, South China University of Technology, GuangZhou 510000, China

xanthones [8]. This low solubility causes challenges for gastrointestinal dissolution and oral bioavailability, hindering the development of pharmaceutical preparations and clinical trials.

Recent studies have focused on the use of natural vegetable oils as solvents for extracting active ingredients from plants. For instance, animal fats have been used to extract carotenoids and capsaicinoids from Sichuan chili [9]. Milk fat (triglycerides), have been hydrolyzed to form natural deep eutectic solvents for the extraction of polycyclic aromatic hydrocarbons from milk powder [10]. Additionally, edible oils have proven effective in extracting flavonoid compounds from propolis [11], and virgin coconut oil has been successfully applied in the extraction of phenolic compounds from mangosteen pericarp [12]. When combined with $scCO_2$ extraction technology, the incorporation of natural vegetable oils as co-extractants has shown promising results in significantly enhancing the extraction efficiency [13, 14]. The primary constituents of vegetable oils are triglycerides, which consist of various fatty acids. These fatty acids typically have long chains containing 14–20 carbon atoms, many feature carbon–carbon double bonds, and medium chains consist of 6–12 carbon atoms [15]. The diverse R groups attached to triglycerides provide distinct properties, influencing their compatibility with certain compounds. Additionally, vegetable oil is a mixture of different triglycerides, free fatty acids, and plant pigments; its impact on the extraction of active substances needs to be considered [16].

Our previous investigations revealed that the utilization of virgin coconut oil (VCO) and palm kernel oil as co-extractants in conjunction with $scCO_2$ can notably increase the extraction efficiency of xanthones from the MP [17, 18]. The xanthones extracted using the $scCO_2$-VCO method also displayed increased bioavailability. Analysis and comparison of the compositions of VCO, palm kernel oil, and other vegetable oils revealed that VCO and palm kernel oil had relatively high concentrations of specific components, notably triglyceride laurate, tricaprylin and tricaprin.

Hence, we hypothesize that the presence of triglyceride laurate, tricaprylin and tricaprin in VCO could be the primary mechanism behind its effectiveness as a co-extractant, potentially enhancing the solubility and extraction efficiency of xanthone. To investigate this aspect, the solubilities of xanthone in tricaprylin and tricaprin were measured. Triglyceride laurate was not chosen for this study because its melting point is approximately 46.5 °C [19, 20], which is semisolid at most experimental temperatures. The solubility data were correlated using the local composition-regular solution theory (LC-RST), Wilson model, and Van't Hoff model to provide comprehensive insights into solute–solvent interactions. The LC-RST model was chosen for its ability to capture local composition effects in non-ideal mixtures, while the Wilson model served as a comparative tool due to its simplicity and wide application in modelling binary systems. The Van't Hoff model was employed to analyse the temperature-dependent solubility and calculate dissolution enthalpy, Gibbs free energy, and entropy. Together, these thermodynamic models offered valuable insights into solute–solvent interactions and dissolution properties, supporting future thermodynamic investigations.

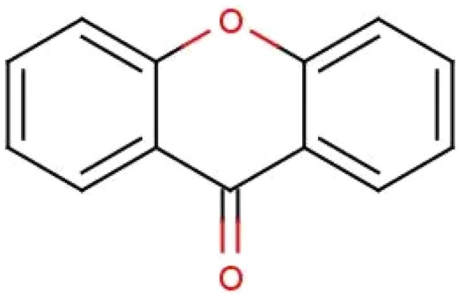

Fig. 1 Chemical structure of xanthone

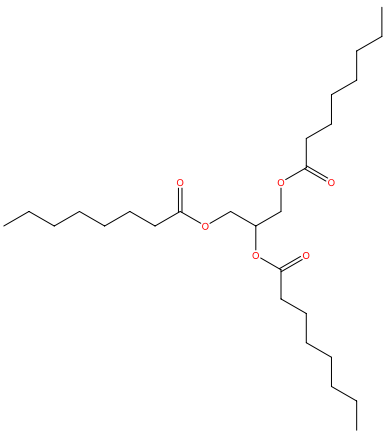

Fig. 2 Chemical structure of tricaprylin

Materials and methods

Materials

Xanthone was procured from McLean Chemical Technology Co., Ltd. Virgin coconut oil (VCO), tricaprin (C10), and tricaprylin (C8) were obtained from Huaxiang Kejie Biotechnology Co., Ltd. All solvents employed in this study were of analytical grade, and the double distilled water was obtained from the water purification equipment (conductivity < 0.5 μs cm^{-1}). The chemical structure and details of the xanthone, C8 and C10 are shown in Figs. 1, 2, 3 and Table 1, respectively.

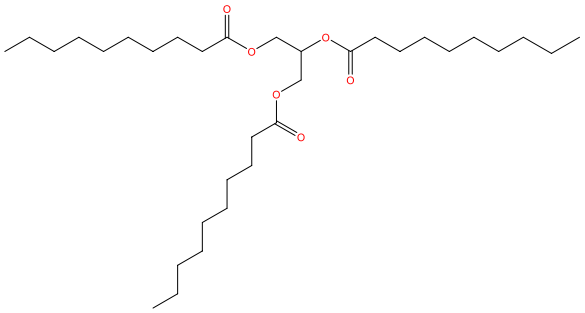

Fig. 3 Chemical structure of tricaprin

Preparation of the precipitated xanthone

To prepare saturated solutions of xanthone in different solvents (C8, C10, and VCO), an excess amount of xanthone was added to airtight glass vials containing 10 mL of each solvent. The vials were placed in a water bath shaker set to 90 °C and shaken for 30 min. The dissolution process was conducted at 90 °C to ensure complete dissolution and obtain sufficient xanthone crystals for subsequent analyses. After shaking, the solutions were allowed to cool to room temperature. The mixtures were then centrifuged to separate the phases, and the supernatant was carefully decanted to collect the xanthone crystals [21]. The samples were analysed via nuclear magnetic resonance (NMR) and X-ray diffraction (XRD); the precipitated xanthone from tricaprin, tricaprylin, and virgin coconut oil was denoted as xanthone-C10, xanthone-C8, and xanthone-VCO, respectively.

Solubility measurements

A shake-flask method was adopted [22] to measure the solubility of xanthone in the solvent used in the study: a mixture of tricaprin (C10, x_2)-tricaprylin (C8, x_3) and VCO. The mixture was prepared at x_2 values ranging from 0 to 1. Excess xanthone was added to an airtight glass vial containing 10 mL of solvent and shaken in a water bath oscillator [23, 24] (SH2-A, Shanghai Juran Instrument Technology Co., Ltd.) at a constant temperature for 6 h. The volume and mass of solvent were recorded for each mixture to allow unit conversions between mg/mL and mole fraction. After 2 h of sedimentation, the concentration of xanthone in the supernatant was measured with an ultraviolet spectrophotometer (UV-1800, Aoyi Instrument Co. Ltd.) at 337 nm. The measurements were continued at 24 h, 48 h, 72 h, 96 h, and 120 h using the same experimental procedure. The constant concentration observed over time was taken as the equilibrium solubility point. The experimental temperatures used were 30 °C, 45 °C, 60 °C and 75 °C (uncertainty = 0.1 °C) under atmospheric pressure (101.2 kPa, uncertainty = 0.1 kPa). The measurements were performed in triplicate. The calibration curves of xanthone in various solvents are illustrated in the supplemental material (Fig. S1).

The mole fraction solubility of xanthone in a mixed-solvent mixture was obtained as follows:

$$x_1 = \frac{\frac{m_1}{M_1}}{\frac{m_1}{M_1} + \frac{m_2}{M_2} + \frac{m_2}{M_2}} \quad (1)$$

where m_1, m_2 and m_3 are the masses of xanthone, C10 and C8, respectively, and where M_1, M_2 and M_3 are the molar masses of xanthone, C10 and C8, respectively [25].

Powder X-ray diffraction (PXRD) analysis

The crystallinity of the standard and precipitated xanthones was analysed using an X-ray powder diffractometer (SmartLab SE, Rigaku). The analysis was conducted under the following conditions: the sample was scanned at a 2θ range between 5° and 90° (40 kV, 40 mA) with a step size of 0.022° and a time per step of 58 s [26].

The calculation of crystallite size is based on the full width at half maximum (FWHM) of diffraction peaks, using the Scherrer formula (2) for calculation [27].

$$D = \frac{K\lambda}{\beta\cos\theta} \quad (2)$$

Where D is the grain size, K is the Scherrer constant, λ is the X-ray wavelength, $\beta$is the full width at half maximum of the diffraction peak, and θ is the diffraction angle.

Table 1 The information of xanthone, tricaprylin, tricaprin and virgin coconut oil

Material	CAS	Sources	Mass fraction purity	Chemical molecular formula	Molar mass (g/mol)
Xanthone	90-47-1	McLean Chemical Technology Co., Ltd	99.757	$C_{13}H_8O_2$	196.2
tricaprylin(C8)	538-23-8	Huaxiang Kejie Biotechnology Co., Ltd	99.00	$C_{27}H_{50}O_6$	498.1
tricaprin (C10)	621-71-6	Huaxiang Kejie Biotechnology Co., Ltd	99.00	$C_{33}H_{62}O_6$	554.8
virgin coconut oil (VCO)	8001-31-8	Huaxiang Kejie Biotechnology Co., Ltd	N/A	N/A	N/A

Fatty acid profiling of VCO in Table S1, purity values of xanthone, tricaprylin and tricaprin were obtained from the supplier

Nuclear magnetic resonance (NMR) analysis

Approximately 10 mg of each sample, including the standard xanthone and precipitated xanthones, was dissolved in dimethyl sulfoxide (DMSO-d6) at a controlled temperature of 24.9 °C for nuclear magnetic resonance (NMR) spectroscopy analysis. Hydrogen (1H) NMR spectra were acquired using a JEOL 400YH NMR spectroscopy system. The parameters set for the analysis included a time domain (TD) of 65 K data points, a receiver gain (RG) of 32, a relaxation delay (D1) of 1 s, a spectral width (SW) of 20 ppm, a spectral width centre (O1p) of 6.175 ppm, 16 scans (NS), and 2 dummy scans (DSs) [28].

Theoretical basis

Thermodynamic model

The standard thermodynamic expression of solid–liquid equilibria (3) was used to describe the solubility of xanthone (x_i) in C8 and C10 [29].

$$ln\frac{1}{x_i} = ln\gamma_i + \frac{\Delta H^f}{RT_m}\left(\frac{T_m}{T} - 1\right) - \frac{\Delta C_p}{R}\left(\frac{T_m}{T} - 1\right) + \frac{\Delta C_p}{R} ln\frac{T_m}{T} \tag{3}$$

where ΔH^f represents the enthalpy of fusion of xanthone, T_m represents the melting temperature of xanthone, R represents the real gas constant, T represents the temperature, ΔC_p represents the change in the heat capacity of xanthone in the liquid and solid states $\left(\Delta C_p = C_{pL} - C_{pS}\right)$, and γ_i represents the activity coefficient of xanthone in C8 and C10. The difference in heat capacities was neglected because the second and third terms in the Eq. 3 have opposite signs, and they approximately cancel each other out, particularly when the difference between T_m and T is small [29]. All the properties used in the calculation are tabulated in Table S2.

Local composition-regular solution and theory (LC-RST) model

The activity coefficient γ was calculated using the LC-RST model, which was improved from regular solution theory (RST) [30]. LC-RST considers local composition theory and temperature [31], and the model is shown as follows:

$$RTln\gamma_k = V_k^L \sum_i \sum_j (A_{ik} - \frac{1}{2}A_{ij})\Phi_i\Phi_j \tag{4}$$

$$\Phi_i = \frac{x_i V_i^L}{\sum_j x_j V_j^L} \tag{5}$$

$$A_{ij} = (\delta_i - \delta_j)^2 + 2l_{ij}\delta_i\delta_j \tag{6}$$

$$l_{ij} = m_{ij}T + b_{ij} \tag{7}$$

where γ_k is the activity coefficient, V_k^L is the molar volume, δ_k is the solubility parameter, Φ_i is the volume fraction of species i, l_{ij} is a fitting parameter and is assumed to have a linear relationship with temperature, m is the slope, and b is the intercept. i, j, and k are the notations for solute and solvents in the solution. The i-j molecular interactions were treated as being unequal, $l_{ij} \neq l_{ji}$.

The molecular interactions were analysed based on the reduction in the objective function value by testing with l_{ij} or l_{ji} one by one. The interaction yielding the lowest value was identified as the dominant interaction and retained. This process was repeated, incrementally increasing the fitting parameters until twelve parameters were included.

Wilson model

The Wilson model considers the theory of local composition, and the activity coefficient is calculated as follows [29]:

$$ln\gamma_k = -\ln(\sum_j^N x_j \wedge_{kj}) + 1 - \sum_i^N \frac{x_i \wedge_{ik}}{\sum_j^N x_j \wedge_{ij}} \tag{8}$$

$$\wedge_{ij} = \frac{V_j^L}{V_i^L}\exp(-\frac{\Delta g_{ij}}{RT}) \tag{9}$$

where V_j^L is the molar volume of component j and Δg_{ij} is the fitting parameter.

The objective function used in this study is as follows:

$$ARDln = \sum_{i=1}^{n} \left| \frac{lnx_{1,i}^{cal} - lnx_{1,i}^{exp}}{lnx_{1,i}^{exp}} \right| \tag{10}$$

where $ARDln$ is the average relative deviation logarithm, cal and exp are the calculated and experimental values, respectively, n is the number of data points, and i is an index for the data in the experiment. All equations were coded in the visual basic application and the solver function in Microsoft Office Excel 365. A sensitivity analysis was conducted by varying key parameters by ± 2% and ± 5% for both the LC-RST and Wilson models, with multiple initial starting points, to ensure that the solutions were not affected by local minima.

Thermodynamic dissolution properties

In this study, the van't Hoff analysis was employed for the thermodynamic analysis of dissolution. The equations are as follows [25]:

$$\Delta_{sol}H_m^o = -R \times \left(\frac{\partial lnx1}{\partial \left(\frac{1}{T} - \frac{1}{T_{mean}} \right)} \right) \quad (11)$$

where $\Delta_{sol}H_m^o$ is the standard molar dissolution enthalpy and T_{mean} is the mean temperature in the temperature range.

$$\Delta_{sol}G_m^o = -RT_{mean} \times intercept \quad (12)$$

where $\Delta_{sol}G_m^o$ is the standard molar Gibbs free energy, and the intercept is obtained from the plot of lnx_1 vs. $(\frac{1}{T} - \frac{1}{T_{mean}})$.

$$\Delta_{sol}S_m^o = \frac{\Delta_{sol}H_m^o - \Delta_{sol}G_m^o}{T_{mean}} \quad (13)$$

$$\%\zeta_H = \frac{\left|\Delta_{sol}H_m^o\right|}{\left|\Delta_{sol}H_m^o\right| + \left|T_{mean}\Delta_{sol}S_m^o\right|} \times 100\% \quad (14)$$

$$\%\zeta_S = \frac{\left|T_{mean}\Delta_{sol}S_m^o\right|}{\left|\Delta_{sol}H_m^o\right| + \left|T_{mean}\Delta_{sol}S_m^o\right|} \times 100\% \quad (15)$$

where $\Delta_{sol}S_m^o$ is the standard molar entropy and $\%\zeta_H$ and $\%\zeta_H$ are the relative contributions of the enthalpy and entropy, respectively, to the Gibbs free energy of dissolution.

Results and discussion

Solubility of xanthone in tricaprin (C10) and tricaprylin (C8)

Effects of solvents

As shown in Fig. 4, xanthone was soluble in C10, C8, the mixture of C10-C18 and VCO. The molecular structure of xanthone includes an aromatic ring, with a degree of hydrophobicity. Similarly, the alkyl chains present in fatty acids are hydrophobic. This shared hydrophobic characteristic indicates a level of molecular compatibility, facilitating the dissolution of xanthone in the solvents used in this study. The solubility of xanthone was greater in C8 than in C10 in the temperature range of 30 °C to 75 °C (Fig. 4). This higher solubility in C8 was attributed to its shorter alkyl chain length, which facilitated better miscibility and minimized the steric hindrance [32, 33]. Additionally, shorter alkyl chain lengths were inversely correlated with hydrophobicity. Thus, C8 exhibited fewer hydrophobic interactions than C10. This reduction in hydrophobic character could result in more favourable interactions with slightly polar compounds, such as xanthone.

When mixtures of C10 and C8 were used, the solubility profile of xanthone exhibited a concave trend, reaching a maximum solubility point at a C10 fraction of $x_2 = 0.36$ from 30 °C to 75 °C (Fig. 5). This result indicated a synergistic effect from the C10–C8 mixture, and the solubility of xanthone was significantly increased with respect to its individual solubility in each fatty acid. Additionally,

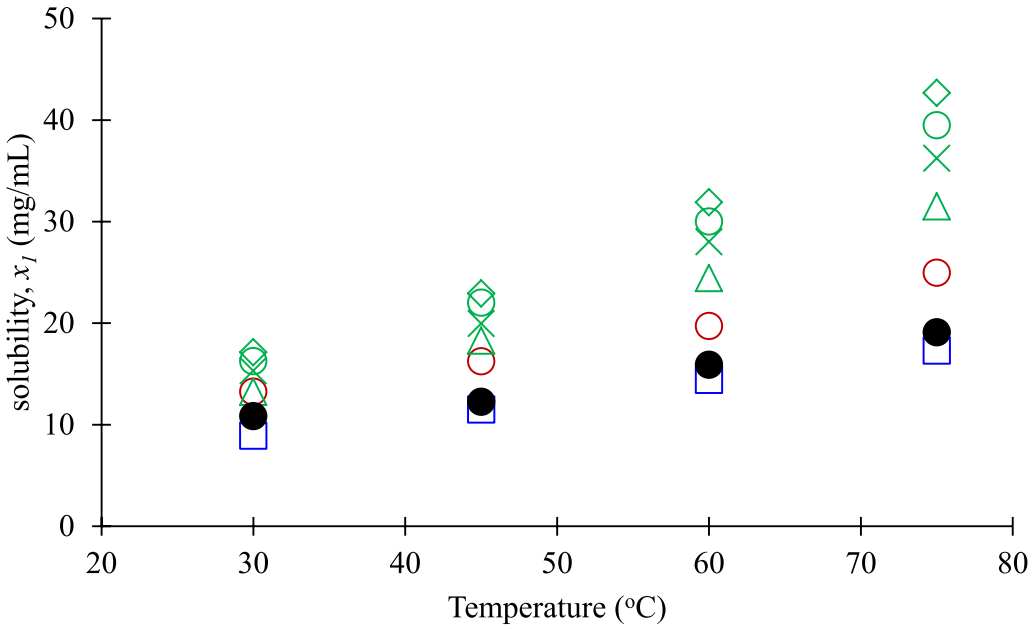

Fig. 4 Solubility of xanthone (1) in a mixture of tricaprin (x_2): tricaprylin (x_3) as a function of temperature. □ (1: 0); △ (0.77: 0.23); ◇ (0.55: 0.45); ○ (0.36: 0.64); × (0.17: 0.83); ○ (0: 1); ● (virgin coconut oil)

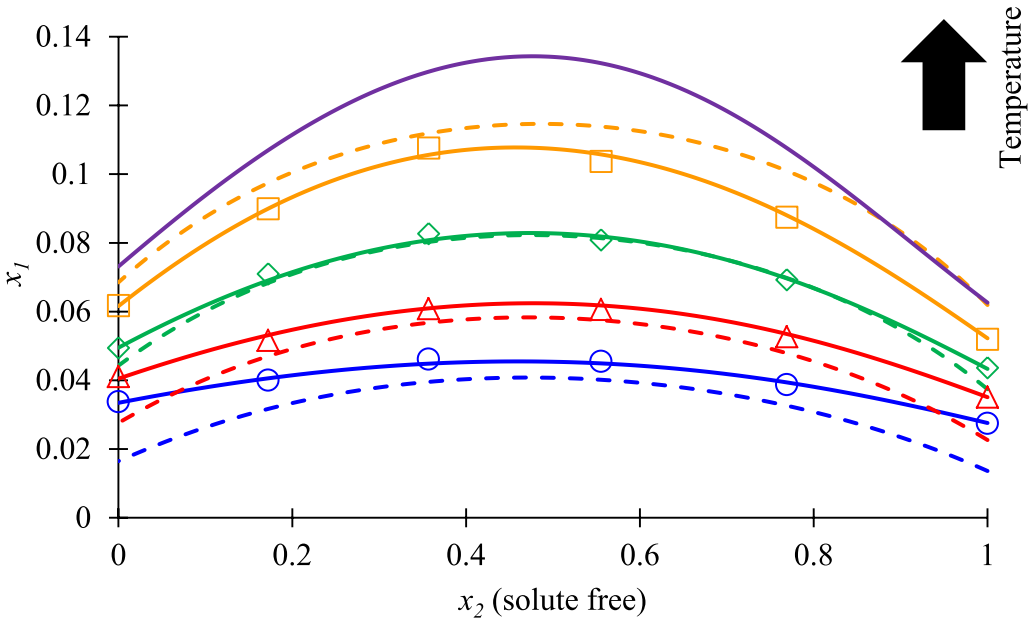

Fig. 5 Solubility profile of xanthone (x_1) in a mixture of tricaprin (x_2): tricaprylin (x_3). Markers: experiment; smoothed line: local composition regular theory model (LC-RST) with significant fitting parameters (l_{23} was removed); dashed line: Wilson model. □: 75 °C (orange); ◇: 60 °C (green); △: 45 °C (red); ○: 30 °C (blue). x_2 (solute free) is the mole fraction of tricaprin (2) in the mixed solvent that is free of xanthone. (Raw data: Table S3). Purple: 90 °C (predicted with LC-RST)

the solubility of xanthone was markedly greater in the C10–C8 mixture than in VCO (Fig. 4), which contains a complex mixture of various fatty acids. The fatty acid composition of virgin coconut oil, detailed in the supplementary material (Table S1), provides insights into the solvent's molecular characteristics, which could influence the solubility of xanthone. The solute–solvent–solvent interaction is discussed in more detail in the next section.

Effect of temperature

As illustrated in Fig. 4, the solubility of xanthone in the tested solvents showed an exponential increase with increasing temperature. Notably, among the solvents evaluated, VCO exhibited the least sensitivity to the temperature changes. The influence of temperature on xanthone solubility became more pronounced at elevated temperatures across the different solvents.

Solubility modelling correlation

Solubility modelling

Figure 5 depicts the correlation of the xanthone solubilities with the LC-RST and Wilson models. Both models could qualitatively provide correlations of the data; however, the LC-RST (4.8×10^{-3} ARDln with l_{23} was removed) was better than the Wilson model (5.6×10^{-2} ARDln). The fitting parameters of both models are listed in Table S4 and Table S6. The results, provided in the supplementary material (Tables S5 and Table S7), confirmed that both models consistently converged to the same minimum. The LC-RST model correlated the data consistently throughout the temperature range; however, the Wilson model underestimated the data from 30 °C to 60 °C and overestimated the data at 75 °C. The LC-RST model provides a more accurate representation of local composition effects and specific molecular interactions in the mixed solvent system. Unlike the Wilson model, which assumes symmetric interactions and lacks temperature dependence, LC-RST handles asymmetric interactions and accounts for temperature-dependent behavior, both of which are crucial in this study. Therefore, the LC-RST model was used to further examine the local interactions among xanthone (1), tricaprin (2) and tricaprylin (3). Additionally, the LC-RST model can be used to predict the solubility of xanthone in a mixture of tricaprin and tricaprylin. The predicted solubility is illustrated in Fig. 5 (purple), showing the similar trend to the experimental data.

As shown in Fig. 6, the highest ARDln value was recorded when all parameters were initially set to zero, and ARDln decreased as nonzero values of the fitting parameters (l_{32}, l_{31}, l_{21}) were introduced. The reduction in ARDln was minimal when more than eight fitting parameters were used in the LC-RST model. In the dissolution of xanthone in tricaprin (2) and tricaprylin (3), the local composition interaction between the solvents, l_{32} and l_{23}, was relatively important; when either l_{32} or l_{23}

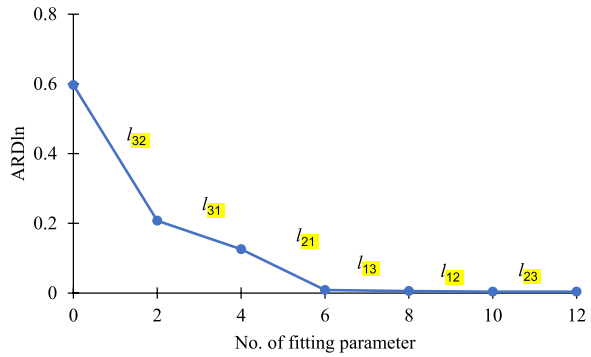

Fig. 6 Xanthone–tricaprin–tricaprylin interaction analysis via the local composition–regular solution theory (LC-RST) model

Table 2 Thermodynamic dissolution properties of xanthone (1) in a mixture of tricaprin (2)-tricaprylin (3) from 30 °C to 75 °C

$\times 2$ (solute free)	$\Delta_{sol}H_m^o$ $\left(\text{kJmol}^{-1}\right)$	$\Delta_{sol}G_m^o$ $\left(\text{kJmol}^{-1}\right)$	$\Delta_{sol}S_m^o$ $\left(\text{kJmol}^{-1}\right)$	ξ_H %	ξ_S %
1	12.48	8.79	0.01	77.17	22.83
0.77	15.92	7.61	0.03	65.70	34.30
0.55	16.14	7.18	0.03	64.30	35.70
0.36	16.64	7.13	0.03	63.63	36.37
0.17	16.06	7.56	0.03	65.40	34.60
0	11.65	8.34	0.01	77.88	22.12

Van't Hoff analysis for xanthone in a mixture of tricaprin and tricaprylin (Figure S2)

was used in the LC-RST model, ARDln decreased from 6.0×10^{-1} to 2.1×10^{-1}. In addition to the interaction of the solvent in the solute environment (l_{31}, l_{21}), the interaction between tricaprylin and xanthone (l_{31}) appeared to be more important than that between tricaprin and xanthone (l_{21}).

Thermodynamic dissolution properties

As shown in Table 2, $\Delta_{sol}H_m^o$ and $\Delta_{sol}G_m^o$ were positive values; thus, the dissolution of xanthone in tricaprin and tricaprylin was a nonideal, endothermic process that was favourable at high temperatures, as shown in Fig. 4. In this study, $\Delta_{sol}H_m^o$ was lower for tricaprin and tricaprylin and increased when these solvents were mixed. This increase indicated that additional energy was required to disrupt the interactions between the molecules in the mixed solvent system. The optimum value of $\Delta_{sol}H_m^o$ was identified between the x_2 (solute free) values of 0.55 and 0.36. The maximum $\Delta_{sol}H_m^o$ was achieved at an x_2 of 0.36. This corresponded to the highest solubility of xanthone in the mixture of tricaprin and tricaprylin. The dissolution of xanthone in this mixture was a nonspontaneous process, as indicated by a positive standard molar Gibbs free energy of dissolution ($\Delta_{sol}G_m^o>0$). The trend of $\Delta_{sol}G_m^o$ over x_2 was concave, and a minimum was observed at an x_2 of 0.36, corresponding to the highest solubility of xanthone in the mixture. Additionally, $\Delta_{sol}S_m^o$ was low for the pure solvent and increased when the two solvents were mixed; thus, the contribution of entropy to solubility became more significant in mixed solvent systems [34] and was in agreement with the findings from this study. The dissolution process of xanthone in tricaprin-tricaprylin was endothermic and was significantly influenced by the entropy effect. This result indicated that xanthone was slightly soluble in the tricaprin–tricaprylin mixture, with the enthalpy contributing more to the standard Gibbs energy than the entropy ($\xi_H > \xi_S$).

Comparative characteristics of xanthone and the precipitated xanthones

Crystallinity analysis

The X-ray powder diffraction (XRPD) patterns of the standard xanthone and precipitated xanthones are shown in Fig. 7.

Figure 7 shows the distinct characteristics of the crystal absorption peak intensities and shapes of xanthone and the precipitated xanthone obtained from the different solvents. The dominant diffraction peaks were observed at approximately 13° and 14° for all types of xanthones. Notably, no new diffraction peaks were observed in the spectra of the precipitated xanthone, indicating that the crystal structure remained unchanged. However, compared with that of the original xanthone, the intensities of the crystalline diffraction peaks of the precipitated xanthones changed.

The diffraction peak of xanthone-C8 exhibited the highest intensity; this intensity was reduced when 40% (v/v) C10 was added and when pure C10 was used. In contrast, the diffraction peak of xanthone-VCO returned to a level similar to that of the original xanthone. In addition, the diffraction peak of xanthone-$x_{2(0.36)}$ also had a relatively high intensity.

Table 3 tabulates the crystallite size of xanthone precipitated from the solvents studied in this study. The crystallite size changed by approximately ± 10% from its original size after precipitation. Among the solvents, xanthone-C8 exhibited the largest crystallite size (71.23 nm), suggesting that tricaprylin promotes more crystal growth compared to the mixture of tricaprin and tricaprylin, which yielded the smallest crystallite size (58.46 nm). These findings show that the physical properties of xanthone can be tailored by selecting appropriate mixture of C10-C8 according to the application.

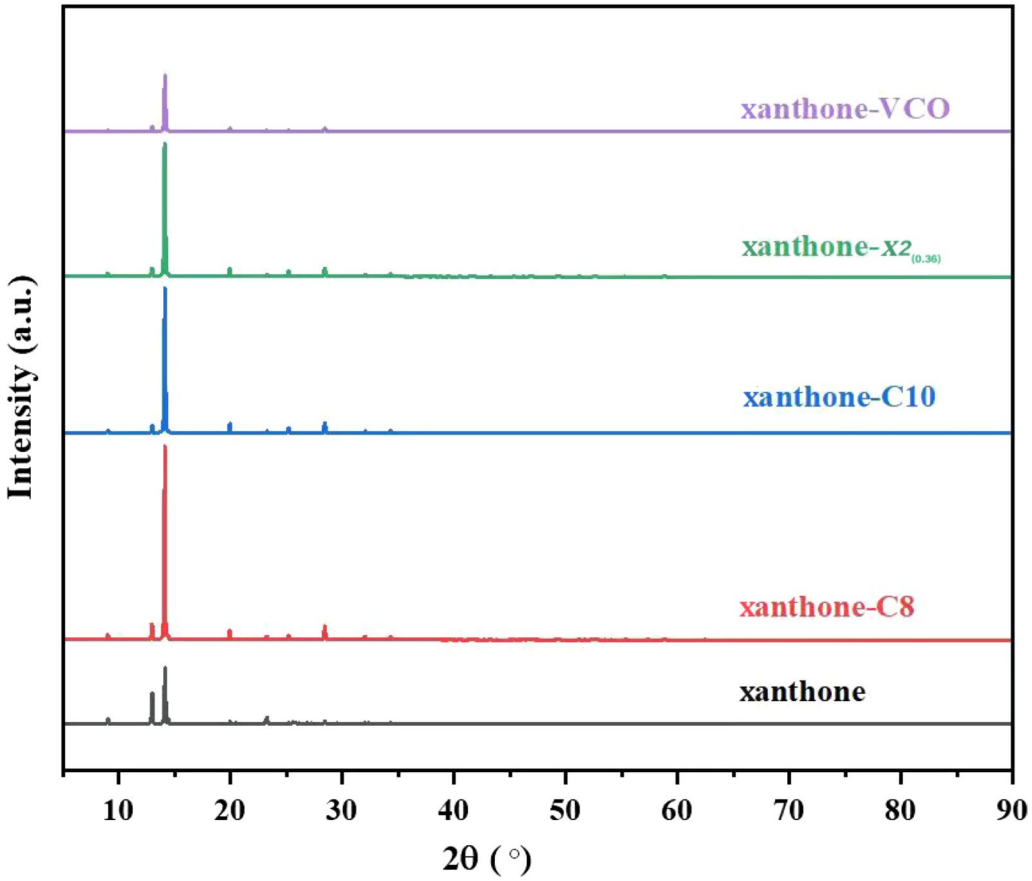

Fig. 7 X-ray diffraction patterns of standard xanthone and precipitated xanthone from tricaprin (C10), tricaprylin (C8), a mixture of C10:C8 (0.36:0.64), and virgin coconut oil

Table 3 X-ray diffraction data in full width at half maximum (FWHM) and crystallite size of the xanthone crystal precipitated from different solvents

Sample	Peak position (2θ)	FWHM (°)	Crystallite size (nm)
Xanthone	14.11	0.12	65.36
Xanthone-C8	14.09	0.11	71.23
Xanthone-C10	14.10	0.13	62.54
Xanthone-$\times 2_{(0.36)}$	14.09	0.14	58.46
Xanthone-VCO	14.11	0.13	60.56

Chemical structure analysis

The ^{1}H NMR spectrum of standard xanthone showed signals in the range of approximately 7.0 ppm to 8.4 ppm (Fig. 8); this result was consistent with the aromatic proton signals expected for xanthone, as reported in the literature review [36]. The observed splitting patterns of doublets and multiplets, were also characteristic of the tricyclic structure of the aromatic protons in xanthone [35]. The proton NMR (^{1}HNMR) spectra of xanthone precipitated from tricaprylin (C8), tricaprin (C10), a mixture of tricaprylin and tricaprin ($x_2 = 0.36$), and virgin coconut oil (VCO) also showed a chemical shift from approximately 7.0 ppm to 8.4 ppm (Figure S3-S6), and the splitting patterns were similar to those of standard xanthone, with the exception of xanthone-C10 and xanthone-VCO; both of these samples showed other signals that were potentially caused by impurities from the solvent environment [36, 37]. These results indicated that the core tricyclic xanthone structure was sustained after precipitation from C10, C8, their mixture and VCO. Therefore, these results have important implications for the isolation and purification of xanthone derivatives from natural sources involving these solvents, enabling further structural characterization or biological evaluation of the isolated compounds.

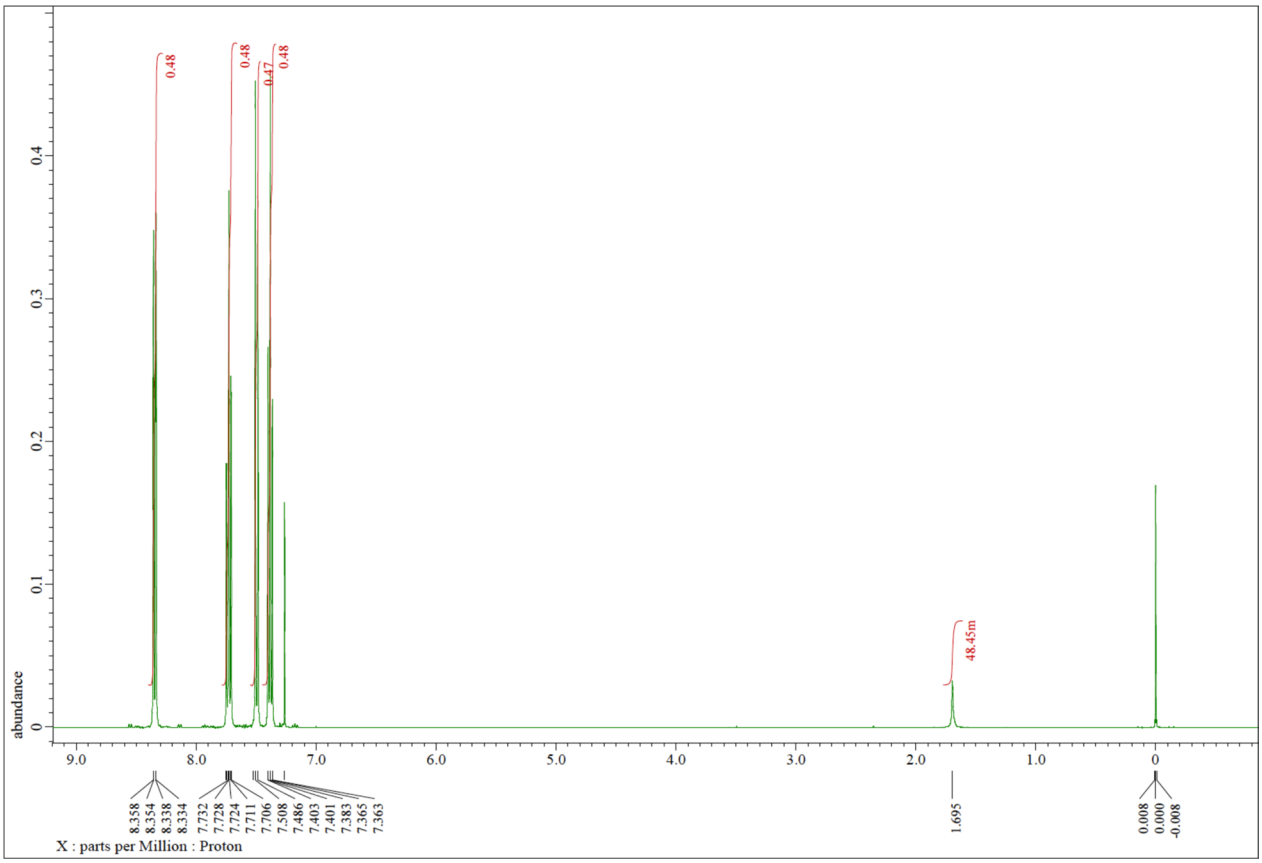

Fig. 8 Nuclear magnetic resonance spectrum of standard xanthone

Conclusion

In this study, the solubility and thermodynamic properties of xanthone in tricaprin (2) and tricaprylin (3), as well as their mixtures, were investigated to understand the role of medium-chain fatty acids in enhancing the solubility and extraction efficiency. The findings revealed that xanthone exhibited the highest solubility in a mixture with a solute-free fraction (x_2) of 0.36 over a temperature range of 30 °C to 75 °C and lower solubility in pure tricaprin and tricaprylin; these results showed a synergistic effect in their mixture.

Additionally, the shorter alkyl chain length and lower viscosity of tricaprylin contributed to the higher solubility of xanthone than of tricaprin. The dissolution of xanthone in tricaprin and tricaprylin was an endothermic and enthalpy-driven process, with the solubility exponentially increasing with temperature.

Local composition interactions included strong interactions between tricaprin and tricaprylin, followed by interactions between tricaprylin and xanthone and between tricaprin and xanthone. Although this study focused on base xanthone, the results provide foundational insights into its interaction with triglyceride-based solvent systems. These findings can be extended to explore the behavior of more hydrophilic xanthone derivatives in future studies. Structural analysis revealed that xanthone maintained its molecular structure after dissolution in tricaprin and tricaprylin; however, changes in crystallinity levels were observed.

These findings provide insights into the use of medium-chain triglycerides as solvents to improve the solubility and bioavailability of hydrophobic compounds such as xanthone. The results from this study highlight the potential of mixed solvent systems in the food and pharmaceutical industries to increase the extraction efficiency and application of bioactive compounds.

Abbreviations

MP	Mangosteen pericarp
$scCO_2$	Supercritical carbon dioxide
C8	Tricaprylin
C10	Tricaprin
VCO	Virgin coconut oil
LC-RST	Local composition- regular solution theory
x_1	Mole fraction of xanthone in the solvent mixture
x_2	Mole fraction of tricaprin in the solvent mixture
x_3	Mole fraction of tricaprylin in the solvent mixture
m_1	Mass of xanthone
m_2	Mass of tricaprin

m_3	Mass of tricaprylin
M_1	Molar mass of xanthone
M_2	Molar mass of tricaprin
M_3	Molar mass of tricaprylin
XRD	X-ray diffraction
D	Grain size
K	Scherrer constant
λ	X-ray wavelength
β	Full width at half maximum of the diffraction peak
θ	Diffraction angle
NMR	Nuclear magnetic resonance
ΔH^f	Enthalpy of fusion of xanthone
T_m	Melting temperature of xanthone
R	Real gas constant
T	Temperature
ΔC_p	Change in the heat capacity of xanthone in the liquid and solid states
γ_k	Activity coefficient
V_k^L	Molar volume
δ_k	Solubility parameter
Φ_i	Volume fraction of species i
l_{ij}	Fitting parameter
M	Slope
b	Intercept
i, j, k	Notations for solute and solvents in the solution
V_j^L	Molar volume of component j
Δg_{ij}	Fitting parameter
$ARDln$	Average relative deviation logarithm
cal, exp	Calculated and experimental values, respectively
n	Number of data points
$\Delta_{sol}H_m^o$	Standard molar dissolution enthalpy
T_{mean}	Mean temperature in the temperature range
$\Delta_{sol}G_m^o$	Standard molar Gibbs free energy
$\Delta_{sol}S_m^o$	Standard molar entropy
$\%\zeta_H, \%\zeta_H$	Relative contributions of the enthalpy and entropy, respectively, to the Gibbs free energy of dissolution

Supplementary Information

The online version contains supplementary material available at https://doi.org/10.1186/s13065-024-01329-6.

Additional file 1.

Acknowledgements
Not applicable.

Author contributions
CRediT author statement Hua Liu: Data curation, Investigation, Methodology, Formal analysis, Writing—Original Draft, Visualization, Resources, Funding acquisition. Johnson Stanslas: Supervision, Writing-Reviewing and Editing. Jiaoyan Ren: Writing-Reviewing and Editing. Norhidayah binti Suleiman: Writing-Reviewing and Editing. Gun Hean Chong: Conceptualization, Supervision, Methodology, Software, Project administration, Resources, Formal Analysis, Writing-Reviewing and Editing.

Funding
This research was financially supported by the Special Innovation Projects for Ordinary Universities in Guangdong Province (no. 2022KTSCX167), the Fund Project of the Laboratory Management Professional Committee of Guangdong Higher Education Association (no. GDJ2022081), and the Ministry of Education Industry University Cooperation Collaborative Education Project of China (no. 220606537282750).

Availability of data and materials
Data is provided within the manuscript or supplementary information files.

Declarations

Ethics approval and consent to participate
Not applicable.

Consent for publication
Not applicable.

Competing interests
The authors declare no competing interests.

Received: 28 August 2024 Accepted: 23 October 2024
Published online: 04 December 2024

References

1. Yuvanatemiya V, Srean P, Klangbud WK, Venkatachalam K, Wongsa J, Parametthanuwat T, Charoenphun N. A review of the influence of various extraction techniques and the biological effects of the xanthones from mangosteen (Garcinia mangostana L) pericarps. Molecules. 2022;27(24):8775.
2. de Mello RFA, de Souza Pinheiro WB, Benjamim JKF, de Siqueira FC, Chiste RC, Santos AS. A fast and efficient preparative method for separation and purification of main bioactive xanthones from the waste of *Garcinia mangostana* L. by high-speed countercurrent chromatography. Arab J Chem. 2021;14(8):103252.
3. Nauman MC, Johnson JJ. The purple mangosteen (*Garcinia mangostana*): defining the anticancer potential of selected xanthones. Pharmacol Res. 2022;175: 106032.
4. Chaiwong N, Phimolsiripol Y, Leelapornpisid P, Ruksiriwanich W, Jantanasakulwong K, Rachtanapun P, Seesuriyachan P, Sommano SR, Leksawasdi N, Simirgiotis MJ, Barba FJ, Punyodom W. Synergistics of carboxymethyl chitosan and mangosteen extract as enhancing moisturizing, antioxidant, antibacterial, and deodorizing properties in emulsion cream. Polymers. 2022;14(1):178.
5. Pothitirat W, Chomnawang MT, Supabphol R, Gritsanapan W. Free radical scavenging and anti-acne activities of mangosteen fruit rind extracts prepared by different extraction methods. Pharm Biol. 2010;48(2):182–6.
6. Konyanee A, Chania P, Chukaew A, Payaka A, Septama AW, Phuwajaroanpong A, Plirat W, Punsawas C. Antiplasmodial potential of isolated xanthones from *Mesua ferrea* Linn. roots: an in vitro and in silico molecular docking and pharmacokinetics study. BMC Complement Med Ther. 2024;24:282.
7. Zarena AS, Udaya SK. Xanthones enriched extracts from mangosteen pericarp obtained by supercritical carbon dioxide process. Sep Purif Technol. 2011;80:172–8.
8. Zhang QW, Lin LG, Ye WC. Techniques for extraction and isolation of natural products: a comprehensive review. Chin Med. 2018;13:20.
9. Zheng B, Wu Y, Wang Y, Li Y. Application of different animal fats as solvents to extract carotenoids and capsaicinoids from Sichuan chili. Foods. 2024;13(10):1478.
10. Shakirova F, Shishov A, Bulatov A. Hydrolysis of triglycerides in milk to provide fatty acids as precursors in the formation of deep eutectic solvent for extraction of polycyclic aromatic hydrocarbons. Talanta. 2022;237: 122968.
11. Pattiram PD, Abas F, Suleiman N, Mohamad Azman E, Chong GH. Edible oils as a co-extractant for the supercritical carbon dioxide extraction of flavonoids from propolis. PLoS ONE. 2022;17(4): e0266673.
12. Sungpud C, Panpipat W, Sae-Yoon A, Chaijan M. Polyphenol extraction from mangosteen (Garcinia mangostana Linn) pericarp by bio-based solvents. Int Food Res J. 2020;27(1):111–20.
13. Shi X, Wu H, Shi J, Xue S, Wang D, Wang W, Cheng A, Gong Z, Chen X, Wang C. Effect of modifier on the composition and antioxidant activity of carotenoid extracts from pumpkin (Cucurbita maxima) by supercritical CO_2. LWT-Food Sci Technol. 2013;51:433–40.

14. Machmudah S, Zakaria, Winardi S, Sasaki M, Coto M, Kusumoto N, Hayakawa K. Lycopene extraction from tomato peel by-product containing tomato seed using supercritical carbon dioxide. J Food Eng. 2012;108:290–6.
15. Geng S, Zhu W, Xie C, Li X, Wu J, Liang Z, Xie W, Zhu J, Huang C, Zhu M, Wu R, Zhong C. Medium-chain triglyceride ameliorates insulin resistance and inflammation in high fat diet-induced obese mice. Eur J Nutr. 2016;55:931–40.
16. Chutia H, Mahanta CL. Green ultrasound and microwave extraction of carotenoids from passion fruit peel using vegetable oils as a solvent: optimization, comparison, kinetics, and thermodynamic studies. Innov Food Sci Emerg Technol. 2021;67: 102547.
17. Kok SL, Lee WJ, Smith RL Jr, Suleiman N, Jom KN, Vangnai K, Sharaai AH, Chong GH. Role of virgin coconut oil (VCO) as co-extractant for obtaining xanthones from mangosteen (*Garcinia mangostana*) pericarp with supercritical carbon dioxide extraction. J Supercritl Fluids. 2021;176: 105305.
18. Lee WJ, Ng CC, Ng JS, Smith R, Kok SL, Hee YY, Lee SY, Tan WK, Zainal Abidin NH, Abdul Halim Lim S, Chong GH. Supercritical carbon dioxide extraction of α-mangostin from mangosteen pericarp with virgin coconut oil as co-extractant and in-vitro bio-accessibility measurement. J Supercritl Fluids. 2019;87:213–20.
19. Feng Y, Wei R, Huang Z, Zhang X, Wang G. Thermal properties of lauric acid filled in carbon nanotubes as shape-stabilized phase change materials. Phys Chem Chem Phys. 2018;20(11):7772–80.
20. Ding L, Wang L, Georgios K, Lü Y, Zhou W. Thermal characterization of lauric acid and stearic acid binary eutectic mixture in latent heat thermal storage systems with tube and fins. J Wuhan Univ Technol Mater Sci Ed. 2017;32(4):753–9.
21. Könczöl Á, Dargó G. Brief overview of solubility methods: recent trends in equilibrium solubility measurement and predictive models. Drug Discov Technol. 2018;27:3–10.
22. Fakhree MA, Ahmadian S, Panahi-Azar V, Acree WE Jr, Jouyban A. Solubility of 2-hydroxybenzoic acid in water, 1-propanol, 2-propanol, and 2-propanone at (298.2 to 338.2) K and their aqueous binary mixtures at 298.2 K. J Chem Eng Data. 2012;57(11):3303–7.
23. Jafari P, Barzegar-Jalali M, Jouyban A. Effect of temperature and composition on solubility and thermodynamics of salicylic acid in aqueous mixtures of betaine-based deep eutectic solvents. Korean J Chem Eng. 2023;40(4):910–24.
24. Pourkarim F, Mirheydari SN, Martinez F, Jouyban A. Solubility of acetaminophen in 1-propanol+ water mixtures at T= 293.2–313.2 K. Phys Chem Liq. 2020;58(4):456–72.
25. Qu J, Zhang Y, Lu D, Wang X. Solubility parameter and solution thermodynamic properties of Form I Trimebutine maleate in six mono-solvents and three binary mixed solvents at different temperatures. J Mol Liq. 2022;367: 120503.
26. Ali A, Chiang YW, Santos RM. X-ray diffraction techniques for mineral characterization: a review for engineers of the fundamentals, applications, and research directions. Minerals. 2022;12(2):205.
27. Doe J. Correlation between full width at half maximum (FWHM) of XRD peak with residual stress on ground surfaces. Mater Sci Eng A. 2024;318:123–34.
28. Li C, Wang Q, Liu Y, Liao B, Zhang X, Chen L, Zhang J, Wang H, Zuo A. A new xanthone isolated from *Garcinia bracteata* and its important effect on NO levels. Nat Prod Res. 2024:1–7.
29. Prausnitz JM, Lichtenthaler RN, de Azevedo EG. Molecular thermodynamics of fluid-phase equilibria. 3rd ed. Englewood Cliffs: Prentice-Hall; 1999.
30. Poling BE, Prausnitz JM, O'Connell JP. The properties of gases and liquids, vol. 5. New York: Mcgraw-Hill; 2001.
31. Lee JL, Chong GH, Kanno A, Ota M, Guo H, Smith RL Jr. Local composition-regular solution theory for analysis of pharmaceutical solubility in mixed-solvents. J Mol Liq. 2024;397: 124012.
32. Jadhav HB, Annapure US. Triglycerides of medium-chain fatty acids: a concise review. J Food Sci Technol. 2023;60(8):2143–52.
33. Fasina O, Hallman H, Craig-Schmidt M, Clements C. Predicting temperature-dependence viscosity of vegetable oils from fatty acid composition. J Americ Oil Chem Soc. 2006;83:899–903.
34. Baranauskaite V, Belysheva M, Pestova O, Anufrikov Y, Skripkin M, Kondratiev Y, Khripun V. Thermodynamic description of dilution and dissolution processes in the $MgCl_2$-CsC_l-H_2O ternary system. Materials. 2021;14(14):4047.
35. Preston JA, Parisi E, Murray B, Tyler AI, Simone E. Elucidating the polymorphism of xanthone: a crystallization and characterization study. Cryst Growth Des. 2024;24(8):3256–68.
36. Abang Heilman DNA, Zamakshshari NH, Yi Mian VJ, Chee Hui AY, Lizazman MA, Ahmad FB. Soulaxanthone, a new xanthone derivative from *Calophyllum soulattri*. Nat Prod Res. 2024:1–7.
37. Cai G, Hu X, Zhang R, Wang J, Fang X, Pang X, Bai J, Zhang T, Zhang T, Lv H, You X, He W, Yu L. Subplenones A-J: dimeric xanthones with antibacterial activity from the endophytic fungus Subplenodomus sp. CPCC 401465. J Nat Prod. 2023;86(11):2474–86.

Publisher's Note